DOE/ET-53088-408 IFSR #408

MHD Modes Driven by Anomalous Electron Viscosity and their Role in Fast Sawtooth Crashes

A.Y. Aydemir
Institute for Fusion Studies
The University of Texas at Austin
Austin, Texas 78712

February 1990

February 13, 1990

MHD Modes Driven by Anomalous Electron Viscosity and Their Role in Fast Sawtooth Crashes

A. Y. Aydemir
Institute for Fusion Studies
The University of Texas at Austin
Austin, Texas 78712

We derive the dispersion relations for both small and large-Δ' modes ($m \geq 2$, and $m = 1$ modes, respectively) driven by anomalous electron viscosity. Under the assumption that the anomalous kinematic electron viscosity is comparable to the anomalous electron thermal diffusivity, we find that the viscous mode typically has a higher growth rate than the corresponding resistive mode. We compare computational results in cylindrical and toroidal geometries with theory and present some nonlinear results for viscous $m = 1$ modes in both circular and D-shaped boundaries and discuss their possible role in fast sawtooth crashes.

I. Introduction

Anomalous electron viscosity has been postulated to be an important consequence of stochastic field lines in magnetic fusion devices.[1] Break up of good magnetic flux surfaces, although an undesirable feature that contributes to anomalous transport, accompanies both small and large scale magnetohydrodynamic activity. It has been observed in studies of major disruptions in tokamaks,[2] where it is generated by nonlinear mode coupling among primary islands. In studies of sawtooth oscillations in toroidal geometry, coupling among secondary island chains that form around the separatrix of a primary $m = 1$ island was also seen to produce large stochastic layers within the $q = 1$ surface.[3] Stochastic field lines are common in reversed field pinches (RFP's), where computational studies again indicate the presence of a large stochastic region in the center of the device due to nonlinear coupling among $m = 1$ modes with different toroidal mode numbers.[4–6]

It is not clear how the effects of stochastic field lines can be self-consistently incorporated into a resistive magnetohydrodynamic (MHD) model. Enhanced perpendicular thermal transport in such fields can be simulated, not entirely accurately, by making use of a large parallel heat conductivity that tends to remove perpendicular temperature gradients in stochastic regions. In low beta, near force-free plasmas, perpendicular gradients of the parallel current, or more specifically, the gradients of $J_{||}/B$, also need to be removed in stochastic layers. As it was postulated by Kaw *et al.*,[1] perpendicular transport of parallel momentum along stochastically wandering fields lines leads to enhanced perpendicular electron viscosity; in parallel Ohm's law, this effect appears as an anomalous current viscosity or hyperresistivity term,

$$E_{||} = \eta J_{||} - \frac{m_e}{ne^2}\mu_e \nabla_\perp^2 J_{||}, \tag{1}$$

which precisely serves the desired purpose of reducing or removing the perpendicular gradients in $J_{||}$. Above, μ_e is the (anomalous) kinematic electron viscosity coefficient.

The form that this hyperresistivity term should take in the parallel Ohm's law so as to preserve certain conservation laws was considered by Boozer[7]; others have obtained estimates for the anomalous viscosity coefficient in the presence of tearing mode turbulence.[8–10] Our emphasis in this article, however, is not the underlying physical mechanisms that may lead to anomalous viscosity; we assume the existence of some physical process that produces

stochastic fields (some examples were given above), and hence anomalous viscosity, and examine the effects produced by such a dissipation mechanism on large scale (low-m) resistive MHD modes. Thus, this article will be in the same spirit as those of Furth *et al.*,[11] and Kaw *et al.*,[1] where such effects were first examined. Furth *et al.* studied the effects on small$-\Delta'$ tearing modes ($m \geq 2$) and showed that the growth rate scales as $\gamma \sim \mu_e^{1/3}$. The effects on the nonlinear evolution of an $m = 2$ island was examined by Kaw *et al.*, who showed that the island grows as $t^{1/3}$ until a critical width is reached, after which it resumes its growth on a resistive time scale.[12] The same work also numerically integrated the linear eigenvalue equations for the tearing layer and showed that large$-\Delta'$ ($m = 1$) modes have a growth rate that scales as $\gamma \sim \mu_e^{1/5}$. More recently, effects of electron viscosity on sawtooth oscillations were examined in transport studies by Ward and Jardin.[13]

In Section II, after reproducing the results of Furth *et al.* for $m = 2$ modes, we derive the dispersion relation for $m = 1$ modes. We show that the linear behavior of the $m = 1$ mode driven by electron viscosity parallels that of the resistive $m = 1$ mode, which was analyzed in detail by Coppi *et al.*[14] In particular, we obtain closed form expressions for the growth rate of $m = 1$ mode in three different regimes where the ideal internal kink is stable, neutral, and unstable. In Section III, computational results from our full MHD code *CTD* is compared with analytic theory. Results from the nonlinear evolution of $m = 1$ modes in toroidal geometry, with circular and D-shaped boundaries, are presented, and their application to fast sawtooth crashes is discussed. Section IV summarizes the results.

II. Dispersion Relations

Since the dissipative terms become important only in a narrow layer around the rational surface where the parallel wave vector $k_{||}$ vanishes, determination of the growth rates typically involves a boundary layer analysis. We will assume that the exterior problem, where ideal MHD equations are valid, has already been solved, providing us with the solutions that the inner layer equations have to satisfy asymptotically.

We obtain the inner layer equations from the reduced MHD equations[15]:

$$\frac{\partial \nabla_\perp^2 \phi}{\partial t} + [\phi, \nabla_\perp^2 \phi] + \nabla_{||} J = 0, \tag{2}$$

$$\frac{\partial \psi}{\partial t} + \nabla_{||} \phi = \eta J - \mu \nabla_\perp^2 J. \tag{3}$$

Above, the brackets are defined by $[f,g] = \mathbf{z}\cdot\nabla_\perp f \times \nabla_\perp g$, and $\nabla_\| f = (\partial f/\partial z) + [f,\psi]$. The parallel current density is given by $J = \nabla_\perp^2 \psi$.

After linearizing, and with usual approximations, the inner layer equations can be put in the form

$$\frac{d^2\phi}{dx^2} + i\frac{x}{x_A}\frac{d^2\psi}{dx^2} = 0, \tag{4}$$

$$\psi + i\frac{x}{x_A}\phi = x_\eta^2 \frac{d^2\psi}{dx^2} - x_\mu^4 \frac{d^4\psi}{dx^4}, \tag{5}$$

where x measures the distance from the rational surface, $x = r - r_s$. The Alfvén layer width, the resistive layer width, and the viscous layer width are given by

$$x_A = \gamma/k'_\|, \tag{6}$$

$$x_\eta^2 = \eta/\gamma, \tag{7}$$

$$x_\mu^4 = \mu/\gamma, \tag{8}$$

respectively. Note that we have let $r/a \rightarrow r$, and $t/\tau_{Hp} \rightarrow t$, where τ_{Hp} is the poloidal Alfvén time given by $\tau_{Hp} = a/v_{A\theta}$, with $v_{A\theta} = B_\theta/(\mu_o\rho)^{1/2}$. In these normalized units, $\eta = \tau_{Hp}/\tau_\eta$, and $\mu = \tau_{Hp}/\tau_\mu$, where the resistive and viscous diffusion times are, in mks units, $\tau_\eta = \mu_o a^2/(\eta)$, and $\tau_\mu = (\omega_p/c)^2 a^4/\mu_e$, respectively. Equation 4 is the vorticity equation, whereas the second equation comes from the parallel Ohm's law. For the remainder of this discussion, we will ignore the the resistive term in Eq. 5 and concentrate on the fourth order viscous term. Together, Eqs. 4,5 comprise a sixth order system for the flux function ψ, or the electrostatic potential ϕ.

Below we solve Eqs. 4, and 5 using Fourier transform techniques. First, modes with $m \geq 2$, which exhibit a finite discontinuity in the first derivative of the flux function, will be examined.

A. Small-Δ' Modes

The solution of the exterior equations for tearing modes is characterized by the quantity Δ', which measures the jump in the derivative of the flux function ψ across the tearing layer[16]:

$$\Delta' = \frac{\psi'(r_s + w/2) - \psi'(r_s - w/2)}{\psi(r_s)}, \tag{9}$$

where we take w to be the width of the tearing layer. Equation 9 represents a contraint that has to be satisfied by the inner layer solution so that it can be asymptotically matched on to the exterior solution.

Before solving Eqs. 4, and 5 with this particular boundary condition, we define an inner variable $y = x/w$, where we take the layer width to be, in anology with the resistive mode,

$$w = \left(x_A x_\mu^2\right)^{1/3}. \tag{10}$$

Then rescaling various quantities as

$$\frac{d\psi}{dx} = \Delta' \frac{d\psi}{dy}, \quad \frac{d^2\psi}{dx^2} = \frac{\Delta'}{w} \frac{d^2\psi}{dy^2}, \quad \text{and}$$
$$\frac{d\phi}{dx} = \frac{1}{w} \frac{d\phi}{dy}, \quad \frac{d^2\phi}{dx^2} = \frac{1}{w^2} \frac{d^2\phi}{dy^2},$$

we rewrite Eqs. 4,5 as

$$\frac{d^2\phi}{dy^2} + iy\Delta' \left(\frac{x_\mu^4}{x_A}\right)^{1/3} \frac{d^2\psi}{dy^2} = 0, \tag{11}$$

$$\frac{x_\mu^2 \Delta'}{x_A} \frac{d^4\psi}{dy^4} + iy \left(\frac{x_\mu}{x_A}\right)^{2/3} \phi + \psi(0) = 0. \tag{12}$$

Note that we made the usual "constant-ψ" approximation, valid for $\Delta' w \ll 1$, and let $\psi(y) \to \psi(0)$ in Eq. 12. At this point, we can obtain an estimate for the growth rate simply by balancing terms in Eqs. 11,12, which gives

$$\gamma \sim \left(\Delta' k_\parallel'\right)^{2/3} \mu^{1/3}. \tag{13}$$

To get a closed form solution to Eqs. 11,12, we formally extend the inner variable y to $(-\infty, +\infty)$, and define the Fourier transforms

$$\begin{Bmatrix} \psi(k) \\ \phi(k) \end{Bmatrix} = \frac{1}{2\pi} \int_{-\infty}^{+\infty} \begin{Bmatrix} \psi(y) \\ \phi(y) \end{Bmatrix} e^{-iky} dy. \tag{14}$$

The techniques used here are similar to those of Pegoraro, and Schep.[17] The transformed equations are:

$$\Delta' \left(\frac{x_\mu^4}{x_A}\right)^{1/3} \frac{dJ}{dk} + k^2\phi = 0, \tag{15}$$

$$\left(\frac{x_\mu}{x_A}\right)^{2/3} \frac{d\phi}{dk} + \frac{x_\mu^2 \Delta'}{x_A} k^2 J = \psi(0)\ \delta(k), \tag{16}$$

where $J = -k^2\psi(k)$ is the transform of the parallel current, and $\delta(k)$ is the delta function. Combining Eqs. 15,16, and rearranging terms, we get

$$\frac{d}{dk}\ \frac{1}{k^2}\ \frac{dJ}{dk} - k^2 J = -a^4 \psi(0)\delta(k), \tag{17}$$

where $a^4 = x_A/(\Delta' x_\mu^2)$. Equation 17 has the solution

$$J(k) = \frac{a^4\ \psi(0)}{2}\ e^{-|k^3|/3}, \tag{18}$$

and $\phi(k)$ is easily found to be:

$$\phi(k) = \frac{\psi(0)}{2}\ \left(\frac{x_A}{x_\mu}\right)^{2/3}\ sgn(k)\ e^{-|k^3|/3}, \tag{19}$$

where *sgn* is the "sign" function. Finally, the growth rate is determined using the constraint equation, Eq. 9, which, in terms of the inner variable y, becomes

$$\int_{-\infty}^{+\infty} J(y)dy = \psi(0). \tag{20}$$

Making use of Eq. 9, Eq. 20 can be put in the form

$$\int_{-\infty}^{+\infty} \frac{\phi''}{y} dy = -i\Delta' \left(\frac{x_\mu^4}{x_A}\right)^{2/3} \psi(0). \tag{21}$$

Using Eq. 19 in Eq. 21 finally yields

$$\frac{x_\mu^2 \Delta'}{x_A} = \pi, \quad \text{or} \tag{22}$$

$$\gamma = \left(\frac{k_\parallel' \Delta'}{\pi}\right)^{2/3}\ \mu^{1/3}. \tag{23}$$

Note that the viscous mode has a weaker dependence on viscosity than the corresponding resistive tearing mode does on resistivity, which has a growth rate that scales as $\gamma \sim \eta^{3/5}$. The growth rate derived here is in agreement with the results of Ref. 11.

B. Large-Δ' Modes

What is meant by small or large-Δ' can be understood easily by considering the relative change in ψ across a boundary layer of width w at $r = r_s$:

$$\frac{\psi(r_s) - <\psi>}{\psi(r_s)} = -\frac{1}{4} w\Delta' + O(w^2), \tag{24}$$

where $<\psi> = [\psi(r_s + w/2) + \psi(r_s - w/2)]/2$. For $w\Delta' \ll 1$ (small Δ'), the relative change as defined above is small and $\psi \simeq <\psi(r)> \simeq \psi(r_s)$. This was the case considered in the section above, where we replaced $\psi(y)$ in the inner layer equations by its value at the rational surface, $\psi(0)$. For $w\Delta' \sim O(1)$ (large Δ'), however, we see that the relative change is of order unity and the "constant-ψ" assumption is no longer justified. This is the case for the solution of the outer layer equations for $m = 1$ internal kink mode, which exhibits a large variation across the boundary layer.[14]

Letting $\Delta' \to 1/w$, and $\psi(0) \to \psi(y)$ in Eqs. (11,12), we obtain the equations appropriate for $m = 1$ modes:

$$\frac{d^2\phi}{dy^2} + iy\frac{1}{a^2}\frac{d^2\psi}{dy^2} = 0, \tag{25}$$

$$\frac{1}{a^4}\frac{d^4\psi}{dy^4} + iy\frac{1}{a^2}\phi + \psi(y) = 0, \tag{26}$$

where now $a = (x_A/x_\mu)^{1/3}$. The boundary conditions for these equations are determined by the exterior solution, which gives[14]:

$$\phi(y) = \frac{i\gamma}{k_\perp} \begin{cases} \xi_\infty + \dfrac{\lambda_H \xi_\infty}{w\pi k'_{||}} \dfrac{1}{y} & y \to -\infty \\ \\ \dfrac{\lambda_H \xi_\infty}{w\pi k'_{||}} \dfrac{1}{y} & y \to +\infty \end{cases} \tag{27}$$

The layer width w is given by Eq. (10), and we define $k_\perp = m/r$. λ_H is the growth rate of the ideal internal kink mode[14,18]:

$$\lambda_H = -\frac{\pi}{r_s^3\, k'_{||}} \int_0^{r_s} g\, dr, \tag{28}$$

where the integrand g is the part of δW that contains the kink drive.

A careful analysis of the Eqs. (25,26) below reveals three distinct roots for the dispersion relation, as in the case of the resistive kink mode. We can obtain one of the roots by simply balancing terms in Eqs. (25,26), which gives

$$\gamma \sim k_{||}'^{4/5} \mu^{1/5}. \tag{29}$$

Again we find that the viscous mode has a weaker dependence on μ than the corresponding resistive mode does on η, for which $\gamma \sim \eta^{1/3}$.

In order to find the full dispersion relation, we Fourier transform Eqs. (25,26). Combining equations, we obtain for the parallel current

$$\frac{d}{dk}\,\frac{1}{k^2}\,\frac{dJ}{dk} - k^2 J = a^4\,\frac{J}{k^2}, \tag{30}$$

Equivalently, we can write the equation in terms of ϕ as

$$\frac{d}{dk}\,\frac{k^2}{a^4+k^4}\,\frac{d\phi}{dk} = k^2\phi. \tag{31}$$

We note that the boundary conditions for ϕ given in Eq. 27 are neither odd, nor even in y. To make the problem more tractable, we notice that if $\phi(k)$ is a solution to Eq. (31) that satisfies the mixed boundary conditons in Eq. (27) (properly transformed to $k-$space), then

$$\phi(k) - i\frac{\gamma}{k_\perp}\frac{\xi_\infty}{2}\,\delta(k) \tag{32}$$

will satisfy Eq. (31) with the following odd boundary conditions:

$$\phi(y) = \frac{i\gamma}{k_\perp}\begin{cases} +\dfrac{\xi_\infty}{2} + \dfrac{\lambda_H \xi_\infty}{w\pi k_{||}'}\,\dfrac{1}{y} & y \to -\infty \\[2ex] -\dfrac{\xi_\infty}{2} + \dfrac{\lambda_H \xi_\infty}{w\pi k_{||}'}\,\dfrac{1}{y} & y \to +\infty \end{cases} \tag{33}$$

The corresponding boundary conditon in $k-$space is

$$\phi(k) = -\frac{\gamma\xi_\infty}{2\pi k_\perp}\,\left\{\frac{1}{k} - \frac{\lambda_H}{wk_{||}'}\,sgn(k)\right\} \quad \text{as } |k| \to 0. \tag{34}$$

Thus, we will look for odd solutions for ϕ that satisfy Eq. (34), or even solutions for J.

From the solution of the $m \geq 2$–problem (Eq. 17)), we know that the solution to Eq. (30) will have the asymptotic behavior

$$J \sim e^{-k^3/3} \text{ for } |k| \to \infty. \tag{35}$$

Thus, we look for solutions of the form

$$J(k) = u(k) e^{-k^3/3}, \tag{36}$$

where $u(k)$ is chosen to satisfy the boundary conditions for $|k| \to 0$. Substituting (36) in (30), we get

$$\frac{d^2u}{dk^2} - 2(k^2 - \frac{1}{k}) \frac{du}{dk} - a^4 u(k) = 0. \tag{37}$$

Neglecting the k^2 term compared to $1/k$ in the coefficient of u' (we are looking for solutions valid for $k \to 0$), this equation can be solved in terms of Whittaker's functions[19]:

$$u(k) = 4a^4 \, e^{-a^2 k} \, k^3 \, U(2, 4, 2a^2 k) \tag{38}$$

where the Kummer's function U is simply given by:

$$U(2, 4, z) = 1/z^2 + 2/z^3. \tag{39}$$

Then, substituting for u in (36) and imposing even symmetry, we obtain

$$J(k) = \left\{ |k| + \frac{1}{a^2} \right\} \, e^{-|a^2 k + k^3/3|}. \tag{40}$$

Using (40), we get for ϕ:

$$\phi(k) = \left\{ \frac{1}{k} + \frac{1}{a^4} + \frac{k}{a^2} \right\} \, e^{-|a^2 k + k^3/3|}. \tag{41}$$

Letting $k \to 0$ in (41) and comparing the result with the boundary conditons for ϕ in (34), we finally obtain the dispersion relation:

$$\frac{1}{a^4} - a^2 = -\frac{\lambda_H}{w \, k'_{||}}. \tag{42}$$

Recall that λ_H is the growth rate of the ideal internal kink mode (Eq. (28)). The layer width w is given by Eq. (10), and we have

$$a^3 = \frac{x_A}{x_\mu} = \frac{1}{k'_{||}} \left(\frac{\gamma}{\mu^{1/5}} \right)^{5/4}. \tag{43}$$

Then, assuming $\gamma \sim \mu^s$ and letting $\mu \to 0$, we have

$$a \to \begin{cases} \infty & \text{for } s = 0 \quad \text{(ideal mode)}, \\ \text{a constant} & \text{for } s = 1/5, \\ 0 & \text{for } s > 1/5. \end{cases} \tag{44}$$

In these three limits, the dispersion relation has the following solutions:

$$\gamma = \begin{cases} \lambda_H & \text{if } \lambda_H > 0, \\ k_{\|}'^{4/5} \mu^{1/5} & \text{if } \lambda_H \sim 0, \\ k_{\|}'^{4/3} \, |\lambda_H|^{-2/3} \, \mu^{1/3} & \text{if } \lambda_H < 0. \end{cases} \tag{45}$$

Note that when the ideal internal kink mode is stable ($\lambda_H < 0$), the viscous $m = 1$ mode behaves like a finite-Δ' mode, which is analogous to the behavior of the resistive $m = 1$ mode.

Below, we compare the viscous and resistive growth rates for $m = 1$, and $m = 2$ modes and discuss the relative importance of modes driven by anomalous electron viscosity.

C. Comparison of Viscous and Resistive Growth Rates

Results of the previous sections are summarized in Table I, where the growth rates of the viscosity-driven modes are compared with those of the corresponding resistive modes.

Letting $\alpha = \mu/\eta$, and comparing the growth rates of viscous and resistive $m = 1$ modes, (for $\lambda_H \sim 0$), we see that for moderate shear ($k_{\|}' \sim 0.1$), the viscous mode dominates for $\alpha \gtrsim 2 \times 10^{-5}$ if we assume $\eta \simeq 10^{-8}$, which is typical of ohmic discharges in large tokamaks. For auxiliary heated tokamaks, the viscous mode dominates for even smaller values of α. At $\eta = 10^{-9}$, we have $\gamma_\mu > \gamma_\eta$ for $\alpha \gtrsim 5 \times 10^{-6}$. Comparisons of $m \geq 2$ modes also lead to similar conclusions. Assuming that the unnormalized value of the kinematic viscosity coefficient is comparable to the anomalous electron thermal diffusivity, which typically has a value of $\chi_e \sim 1 m^2/sec$, then for typical large tokamak discharges, $\mu/\eta \sim 10^{-4}$, in our nondimensional units. Thus, linear growth rates of the viscous modes, both for $m = 1$, and $m = 2$, would be typically higher under these conditions than those of the resistive modes. Nonlinearly, Kaw *et al.* showed that $m = 2$ modes enter the typical Rutherford regime after the island width exceeds a critical width, with only the resistivity playing a

major role in the subsequent evolution of the island.[1] However, since $m = 1$ islands do not exhibit a Rutherford regime and continue to grow exponentially far into the nonlinear phase, anomalous electron viscosity is expected to continue to play a role in the nonlinear evolution of the island if $\gamma_\mu > \gamma_\eta$ initially. These questions are further addressed in the next section.

III. Computational Results

We have modified our three dimensional, toroidal, nonlinear MHD code, *CTD*,[3],[4] to incorporate the anomalous viscosity term into the Ohm's law. The equations solved by *CTD*, written in nondimensional form, are:

$$\frac{\partial \mathbf{u}}{\partial t} + \mathbf{u}\cdot\nabla\mathbf{u} = \mathbf{J}\times\mathbf{B} - \nabla p + \mu_i\nabla^2\mathbf{u}, \tag{46}$$

$$\frac{\partial \mathbf{A}}{\partial t} = \mathbf{u}\times\mathbf{B} - \eta\mathbf{J} - \nabla\times\mu\nabla\times\mathbf{J}, \tag{47}$$

$$\frac{\partial p}{\partial t} + \mathbf{u}\cdot\nabla p = -\Gamma p\nabla\cdot\mathbf{u} + \frac{\kappa_{\|}}{B^2}(\mathbf{B}\cdot\nabla)^2 p + \nabla\cdot(\kappa_{\perp}\nabla p) + (\Gamma-1)\eta J^2, \tag{48}$$

$$\mathbf{B} = \nabla\times\mathbf{A} \text{ and } \mathbf{J} = \nabla\times\mathbf{B}. \tag{49}$$

The anomalous electron viscosity, or hyperresistivity term, $\nabla\times\mu\nabla\times\mathbf{J}$, in the Ohm's law, Eq. (47), is written with an isotropic coefficient because of the difficulty of isolating the parallel component of the current in a three dimensional geometry. Note that hyperresistivity coefficient μ is to be distinguished from the ion viscosity μ_i appearing in the momentum equation, Eq. (46).

The Lundquist number S, ratio of the resistive diffusion time to the poloidal Alfvén time, is given by $S = 1/\eta(0)$, where $\eta(0)$ is the value of resistivity on axis. $\kappa_{\|}$, and $\kappa_{\perp}$ are the parallel and perpendicular thermal conductivites, respectively, and Γ is the ratio of specific heats.

The variables have been normalized as follows:

$$t \to \frac{t}{\tau_{Hp}}, \quad \mathbf{r} \to \frac{\mathbf{r}}{a},$$

$$\mathbf{B} \to \frac{\mathbf{B}}{B_{po}}, \quad \mathbf{u} \to \frac{\mathbf{u}}{u_{Hp}}, \quad p \to \frac{p}{B_{po}^2/\mu_o}, \text{ where}$$

$$u_{Hp} = \frac{B_{po}^2}{\sqrt{\rho_o\mu_o}}, \quad \tau_{Hp} = \frac{a}{u_{Hp}}, \quad \tau_R = \frac{\mu_o a^2}{\eta_o}, \quad S = \frac{\tau_R}{\tau_{Hp}}.$$

B_{po} is a characteristic poloidal field strength, and a is the minor radius. The transport coefficients in the pressure equation are normalized as $\kappa_{\perp} = \tau_{Hp}/\tau_{\kappa_{\perp}}$, and $\kappa_{\|} = \tau_{Hp}/\tau_{\kappa_{\|}}$, where $\tau_{\kappa_{\perp}} = a^2/\kappa_{\perp o}$, and $\tau_{\kappa_{\|}} = a^2/\kappa_{\|o}$. $\kappa_{\perp o}$, and $\kappa_{\|o}$ are the dimensional values of the coefficients. As stated earlier, normalized electron viscosity is given by $\mu = \tau_{Hp}/\tau_{\mu}$, where $\tau_{\mu} = (\omega_p/c)^2 a^4/\mu_e$.

In order to treat noncircular geometries, *CTD* has been modified to use conformal coordinates.[20,21] A noncircular domain in the (r,θ) (poloidal) plane bounded by the curve

$$x(\alpha) = \cos(\alpha + \delta\sin(\alpha)),$$
$$y(\alpha) = \kappa\sin(\alpha)),$$

is mapped onto a unit disk in the coordinate system (ρ,ω) using the conformal transformation

$$x(\rho,\omega) = \Delta + \sum_{m=1} a_m \rho^m \cos(m\omega),$$
$$y(\rho,\omega) = \sum_{m=1} a_m \rho^m \sin(m\omega).$$

Above, κ and δ are the ellipticity and triangularity, respectively. Δ represents the toroidal shift in (r,θ) coordinate system and is used to align the magnetic axis with $\rho = 0$. The angles α and θ are related by $\theta = \arctan(y(\theta(\alpha))/x(\theta(\alpha)))$. The major advantage of this coordinate system is that a code written in (r,θ,ζ) toroidal polar coordinates can be easily modified for conformal cordinates. Redefining the state variables as

$$(\tilde{u}_\rho, \tilde{u}_\omega, \tilde{u}_\zeta) = (hu_\rho, hu_\omega, u_\zeta),$$
$$(\tilde{A}_\rho, \tilde{A}_\omega, \tilde{A}_\zeta) = (hA_\rho, hA_\omega, A_\zeta), etc.,$$

and casting the equations in terms of these new $\tilde{}$-variables, the differential operators largely retain their polar coordinate forms, except for factors of h^2 in a small number of terms. Here h is the scale factor in the length element $ds^2 = h^2(d\rho^2 + \rho^2 d\omega^2)$ and is given by

$$h^2 = \frac{1}{\rho^2}\left[\left(\frac{\partial x}{\partial \omega}\right)^2 + \left(\frac{\partial y}{\partial \omega}\right)^2\right].$$

The computational details of conformal coordinate system used in *CTD* will be published elsewhere. Conformal coordinates have the disadvantage of requiring a large number of modes to describe highly deformed boundaries. There are more compact formulations[22] that we are presently examining. Unfortunately, their implementation is not as straight forward, and their computational merits in nonlinear calculations are not clear.

Even for circular boundaries, we use conformal coordinates to align the coordinate and magnetix axes in order to improve numerical accuracy and stability near the axis. In this

case, only three terms in the conformal expansions are sufficient for convergence with toroidal shifts of order 10%. Alternatively, a bilinear (Moebius) tranformation given by Goedbloed[23] can be used for this purpose, but is not implemented in *CTD*.

Below we first do linear studies of $m = 1$, and $m \geq 2$ modes, in cylindrical and toroidal geometries, and verify that scaling of the computationally obtained growth rates with electron viscosity agree with the analytic theory of previous sections. Then in the next subsection, we discuss the role of nonlinear viscous $m = 1$ mode in fast sawtooth crashes, giving examples from both circular and noncircular geometries.

A. Linear Studies with *CTD*

For our linear and nonlinear studies, we have chosen the well-known equilibrium safety factor profile $q(\rho) = q_o\{1 + \rho^{2\lambda}[(q_l/q_o)^{\lambda} - 1]\}^{1/\lambda}$, with three free parameters: q_o (q on axis), q_l (q at the edge) , and λ, which determines sheer. Unless otherwise indicated, we will have $q_l = 3$, and $\lambda = 4$. An aspect ratio of $R_o/a = 3$ will be used throughout. Finite$-\beta$ effects will not be investigated here, and average toroidal beta will be fixed at an arbitrary value of $\beta = 0.08\%$. The linear results presented in this section will all have circular boundaries.

Figure 1 shows the scaling of the growth rate with electron viscosity for finite-Δ' modes in cylindirical and toroidal geometries. Here we use $q_o = 1.2$. Toroidal calculations are for $n = 2$ modes, dominated by the $m/n = 3/2$ harmonic, whereas the cylindrical calculations are for $m/n = 3/2$ only. In both cases, the growth rate scales as $\gamma \sim \mu^{1/3}$, in agreement with the theory of the previous section. Note that the growth rate is reduced by toroidal effects, as it is commonly observed for tearing modes. Since the global behavior of the mode is determined by the ideal MHD solution in the exterior region, profiles for the eigenfunctions obtained here for the viscous modes are quite similar to those seen in purely resistive calculations.

Results of a similar scaling study for large-Δ' modes are shown in Fig. 2. Here $q_o = 0.9$, and we examine the $n = 1$ mode in toroidal geometry, dominated by the $m/n = 1/1$ harmonic, and a pure $m/n = 1/1$ mode in cylindrical geometry. In both cases, the growth rate scales as $\gamma \sim \mu^{1/5}$. Fig. 3 shows the radial eigenfunctions for the $m/n = 1/1$, and $m/n = 2/1$ modes from the toroidal calculation, which had $\eta = 10^{-8}$, and $\mu = 10^{-10}$. Note that the radial velocity profile for $m = 1$ exhibits a step function-like behavior characteristic of that mode. Since the mode is dominated by the $m/n = 1/1$ harmonic, the $m = 2$

eigenfunction displays a large structure at the $q = 1$ surface rather than at its own resonance layer at the $q = 2$ surface.

Both scaling studies were done with a constant resistivity of $\eta = 10^{-8}$. As seen in Figs. 1, and 2, in linear calculations the predicted scalings hold even when the viscosity is three orders of magnitude smaller than resistivity. In fact, comparing the analytic expressions for the growth rates of the resistive and viscous modes, we expect the viscous modes to dominate over the corresponding resistive ones even in the numerically inaccessible region $\mu/\eta \ll 10^{-3}$, as it was discussed in Section 2.C.

In the next section, we investigate the nonlinear evolution of $m = 1$ modes in toroidal geometry with both circular and shaped cross sections.

B. Nonlinear Studies with *CTD*: Fast Sawtooth Crashes

Long after their discovery,[24] our understanding of sawtooth oscillations is still far from complete. Although we demonstrated that many of the experimental features can be explained in terms of the Kadomtsev reconnection process,[3] fast sawtooth crashes observed on large tokamaks,[25] and sawtooth oscillations in low$-q_o$ devices where q_o remains below unity throughout the sawtooth cycle,[26] are still not understood. The difficult problem of understanding sawteeth without full reconnection is beyond the scope of this paper. But here we would like to examine the role of viscosity-driven modes in fast sawtooth crashes.

A possible explanation for the fast crashes was offered in terms of a pressure driven ideal internal kink mode.[27–29] However, these modes are highly sensitive to the details of the $q-$profile; in particular, they require very weak shear within the $q = 1$ surface. Since our self-consistent simulations indicate that q_o tends to fall below one during the sawtooth ramp,[3] whether these ideal modes can play a role in fast crashes is no longer clear. Here, we offer an alternative explanation in terms of a viscosity-driven $m = 1$ mode.

In previous sections we saw that, if we assume $\mu_e \sim \chi_e$, then the viscous $m = 1$ mode generally has a larger growth rate than the $m = 1$ resistive kink mode. In addition, local value of the electron viscosity coefficient around rational surfaces and separatrices of islands is expected to be even larger than this global value given by $\mu_e \sim \chi_e$. This further enhancement of μ_e can be due to stochastic layers that develop because of both small scale MHD fluctuations and nonlinear interaction of modes with nearby rational surfaces. Without spec-

ifying the exact cause and nature of this anomalous enhancement, which is beyond the scope of this paper, below we study its nonlinear consequences.

Figure 4 shows the evolution of the temperature contours from a nonlinear, toroidal calculation of viscous $n = 1$ mode, which was dominated by the $m/n = 1/1$ harmonic. The initial equilibrium had $q_o = 0.95, q_l = 3$, and $\lambda = 2$. Here we had $\eta = 10^{-8}$, and $\mu = 10^{-10}$ in normalized units. This value of μ represents an enhancement by a factor of $10 - 100$ over its global value given by $\mu_e \sim \chi_e$. Up to 48 Fourier modes (with $n_{max} = 4$) and 765 radial grid points were used in this calculation. The initial helical shift of the temperature peak, and the subsequent achievement of poloidal symmetry, is characteristic of this mode and is routinely seen also in purely resistive calculations.[3] The time scale, however, is significantly different in this case. The sawtooth crash time, as measured from the beginning of the shift to the time when poloidal symmetry is seen, is an order of magnitude shorter than a corresponding purely resistive calculation would yield. (Since purely resistive nonlinear calculations at realistic value of resistivity are computationally difficult, the resistive crash time for $\eta = 10^{-8}$ is obtained by extrapolating from calculations done at $\eta \sim 10^{-6}$.) In dimensional units, the crash time is on the order of $100\mu sec$, comparable to the fast collapse times reported by large tokamaks.[25]

Similar results are obtained in a noncircular geometry, as shown in Fig. 5. The D-shaped equilibrium used here has an elongation of 1.6 and triangularity of 0.4, parameters similar to those of JET. The same $q-$profile as in the circular run is used, with $\mu = 10^{-9}$, and $\eta = 10^{-8}$. Here we used 81 modes and 250 radial grid points. The crash time is again much faster than a purely resistive mode would give under the same conditions. Note that the deformation of the hot spot is much more pronounced here than in the circular run. Very early in the crash it assumes a crescent shape, the two ends of which almost, but not quite, connect to form a hot, elliptical annulus at the end of the crash, leading to a hollow temperature profile.

Using the $m = 1$ resistive kink as the driving mechanism for the crash, Kadomtsev heuristically obtained a Sweet-Parker scaling for the crash time[30]:

$$\tau_c = (\tau_H^* \tau_\eta)^{1/2}, \tag{50}$$

where τ_H^* is the poloidal Alfvén time based on the helical field $B^* = \mathbf{k} \cdot \mathbf{B}/|\mathrm{k}|$, and τ_η is the resistive diffusion time, $\tau_\eta = \mu_o a^2/\eta$. This scaling where $\tau_c \sim \eta^{1/2}$ was confirmed in nonlinear

calculations.[3]

Using a similar heuristic argument, we easily obtain the following crash-time scaling with electron viscosity:

$$\tau_c = \left(\tau_H^{*3}\tau_\mu\right)^{1/4}, \tag{51}$$

where the viscous diffusion time is given by $\tau_\mu = (\omega_p/c)^2 a^4/\mu_e$. Note that the crash time based on the viscous mode has a much weaker dependence on the dissipation coefficient ($\tau_c \sim \mu_e^{1/4}$). Thus, variations in μ of as large as a few orders of magnitude will not significantly change τ_c; we would still obtain "fast crashes" even with $\mu \sim 10^{-12}$, a value implied by the assumption $\mu_e \sim \chi_e$.

IV. Conclusions

Incorporating electron viscosity in a generalized Ohm's law, we investigated its effects on low mode number MHD modes. We reproduced earlier results for $m \geq 2$ modes where "constant-ψ" assumption is valid and extended the analysis to $m = 1$ modes where that assumption breaks down. For the finite$-\Delta'$ modes ($m \geq 2$), we found that the growth rate scales as $\mu^{1/3}$. For the large$-\Delta'$ modes ($m = 1$), the dispersion relation has three branches, anolagous to the behavior of the resistive $m = 1$ mode: When the ideal internal kink mode is robustly unstable, we have $\gamma = \lambda_H$, where λ_H is the growth rate of the ideal mode. When the ideal kink is near marginal stability, as is the case under typical conditions, $\gamma \sim \mu^{1/5}$. When the ideal mode is stable ($\lambda_H < 0$), then the mode has a "tearing" character, and the growth rate again scales as $\mu^{1/3}$.

If we assume that, like many other transport coefficients, electron viscosity is also anomalous and has a value comparable to that of the anomalous electron thermal diffusivity, then the viscosity driven modes typically have higher growth rates than the corresponding resistive modes in present fusion devices. Nonlinearly, earlier works had shown that viscosity-driven $m \geq 2$ islands resume their secular growth on a resistive time scale after the island reaches a critical width; thus, for these modes, nonlinear effects of anomalous viscosity are not expected to be important. Their nonlinear behavior is not investigated in this article. However, for $m = 1$ modes, which do not have a "Rutherford regime", significance of the viscous drive persists in the nonlinear phase.

In earlier nonlinear toroidal calculations with *CTD*, we had found that, although most experimentally observed features of tokamak sawtooth oscillations can be explained in terms of the nonlinear evolution of an $m = 1$ resistive kink mode (Kadomtsev reconnection model), the time scale for the fast sawtooth collapse could not be explained in terms of a purely resistive model. Nonlinear calculations of a viscous $m = 1$ mode, however, lead to a much shorter crash time with a similar collapse mechanism; anomalous electron viscosity-driven $m = 1$ modes may indeed explain the fast crashes seen on large tokamaks.

Central to this article is the assumption that magnetic stochasticity produced by low level MHD fluctuations, and nonlinear or toroidal coupling of low mode number MHD modes, lead to an anomalous electron viscosity of the order of the anomalous electron thermal diffusivity. Quantitative predictions of anomalous μ_e produced by such physical effects, or others not described here, should be a fruitful area of future research.

V. Acknowledgements

The author greatfully acknowledges countless fruitful discussions with Wolfgang Stodiek, who has been the driving force behind this work since its beginning.

* Work supported by the U.S. Department of Energy under contract No. DE-FG05-80ET-53088.

Table I. Comparison of the growth rates for viscous and resistive modes.

Mode Number	Viscous Modes	Resistive Modes[14,16]	Comments
$m = 1$	λ_H	λ_H	$\lambda_H > 0$
	$k_{\|\|}'^{4/5}\mu^{1/5}$	$k_{\|\|}'^{2/3}\eta^{1/3}$	$\lambda_H \sim 0$
	$k_{\|\|}^{4/3}\lvert\lambda_H\rvert^{-2/3}\mu^{1/3}$	$\left\{\frac{\Gamma(5/4)}{\Gamma(-1/4)\lambda_H}\right\}^{4/5} k_{\|\|}'^{6/5}\eta^{3/5}$	$\lambda_H < 0$
$m \geq 2$	$\left\{\frac{k_{\|\|}'\Delta'}{\pi}\right\}^{2/3}\mu^{1/3}$	$\left\{\frac{1}{2\pi}\frac{\Gamma(1/4)}{\Gamma(3/4)}\Delta'\right\}^{4/5} k_{\|\|}'^{2/5}\eta^{3/5}$	

Figures

FIG. 1. Scaling of the growth rate with electron viscosity for $m \geq 2$ modes: a) toroidal $n = 2$ mode, b) cylindrical $m/n = 3/2$ mode.

FIG. 2. Scaling of the growth rate with electron viscosity for the $m = 1$ mode: a) toroidal $n = 1$ mode, b) cylindrical $m/n = 1/1$ mode.

FIG. 3. Radial eigenfunctions for the viscous $n = 1$ mode (from a toroidal calculation). Only the $m/n = 1/1$, and $m/n = 2/1$ harmonics are shown.

FIG. 4. Evolution of the temperature (pressure) contours during a sawtooth collapse driven by a viscous $n = 1$ ($m/n = 1/1$) mode (circular boundary). Times are in units of poloidal Alfvén time.

FIG. 5. Evolution of the temperature (pressure) contours during a sawtooth collapse driven by a viscous $n = 1$ ($m/n = 1/1$) mode. The geometry is noncircular, with $\kappa = 1.6$, and $\delta = 0.4$. The $q-$ profile is the same as that of the circular geometry run shown in Fig. 4.

References

[1]P. K. Kaw, E. J. Valeo, and P. H. Rutherford, Phys. Rev. Lett, **43**, 1398 (1979).

[2]B. A. Carreras, H. R. Hicks, J. A. Holmes, and B. V. Waddell, Phys. Fluids **23**, 1811 (1980).

[3]A. Y. Aydemir, J. C. Wiley, D. W. Ross, Phys. Fluids B **1**, 774 (1989).

[4]A. Y. Aydemir and D. C. Barnes, Phys. Rev. Lett. **52**, 930 (1984).

[5]D. D. Schnack, E. J. Caramana, and R. A. Nebel, Phys. Fluids **28**, 321 (1985).

[6]J. A. Holmes, B. A. Carreras, P. H. Diamond, and V. E. Lynch, Phys. Fluids **31**, 1166 (1988).

[7]A. H. Boozer, J. Plasma Physics **35**, 133 (1986).

[8]A. Bhattacharjee, and E. Hameiri, Phys. Rev. Lett. **57**, 206 (1986).

[9]H. R. Strauss, Phys. Fluids **29**, 3668 (1986).

[10]G. G. Craddock, submitted to Phys. Fluids (January 1990).

[11]H. P. Furth, P. H. Rutherford, and H. Selberg, Phys. Fluids **16**, 1054 (1973).

[12]P. H. Rutherford, Phys. Fluids **16**, 1903 (1973).

[13]D. J. Ward, S. C. Jardin, Nucl. Fusion **29**, 905 (1989).

[14]B. Coppi, R. Galvao, R. Pellat, M. Rosenbluth, and P. Rutherford, Sov. J. Plasma Phys. **2**, 533, (1976), [Fiz. Plazmy **2**, 961 (1976)].

[15]H. R. Strauss, Phys. Fluids **19**, 134 (1976).

[16]H. P. Furth, J. Killeen, and M. N. Rosenbluth, Phys. Fluids **6**, 459 (1963).

[17]F. Pegoraro, and T. Schep, Plasma Phys. and Controlled Fusion **28**, 647 (1986).

[18]M. N. Rosenbluth, R. Y. Dagazian, and P. H. Rutherford, Phys. Fluids **16**, 1894 (1973).

[19]F. Oberhettinger, in *Handbook of Mathematical Functions*, eds. M. Abramowitz and I. A. Stegun (Dover-New York, 1968), p. 555.

[20]J. Goedbloed, Phys. Fluids **25**, 2062 (1983).

[21]H. R. Strauss, D. A. Monticello, and J. Manickam, Bull. Am. Phys. Soc. **32**, 1773 (1987), and Nucl. Fusion **29**, 320 (1989).

[22]S. P. Hirshman, H. K. Meier, Phys. Fluids **28**, 1387 (1985).

[23]J. Goedbloed, Phys. Fluids **25**, 858 (1982).

[24]S. von Goeler, W. Stodiek, and N. Sauthoff, Phys. Rev. Lett. **33**, 1201 (1974).

[25]D. J. Campbell and JET Group, in *Proceedings of the Twelfth European Conference on Controlled Fusion and Plasma Physics, Budapest, Hungary, 1985*, edited by L. Pócs and A. Montvai (European Physical Society, Petit-Lancy, Switzerland, 1985)., vol. 1, p. 130; K. McGuire and TFTR Group, *ibid.*, Vol. 1 P. 134.

[26]H. Soltwisch, W. Stodiek, J. Manickam, and J. Schlüter, in *Plasma Physics and Controlled Nuclear Fusion Research, 1986*, Proceedings of the 10th International Conference, Kyoto, 1986, (IAEA, Vienna, 1987), Vol. I, p. 263.

[27]J. A. Wesson, Plasma Phys. Controlled Fusion **28**, 243 (1986).

[28]R. J. Hastie, T. C. Hender, B. A. Carreras, L. A. Charlton, and J. A. Holmes, Phys. Fluids **30**, 1756 (1987).

[29]A. Y. Aydemir, Phys. Rev. Lett. **59**, 649 (1987).

[30]B. B. Kadomtsev, Fiz. Plazmy **1**, 710 (1975) [Sov. J. Plasma Phys. **1**, 389 (1975)].

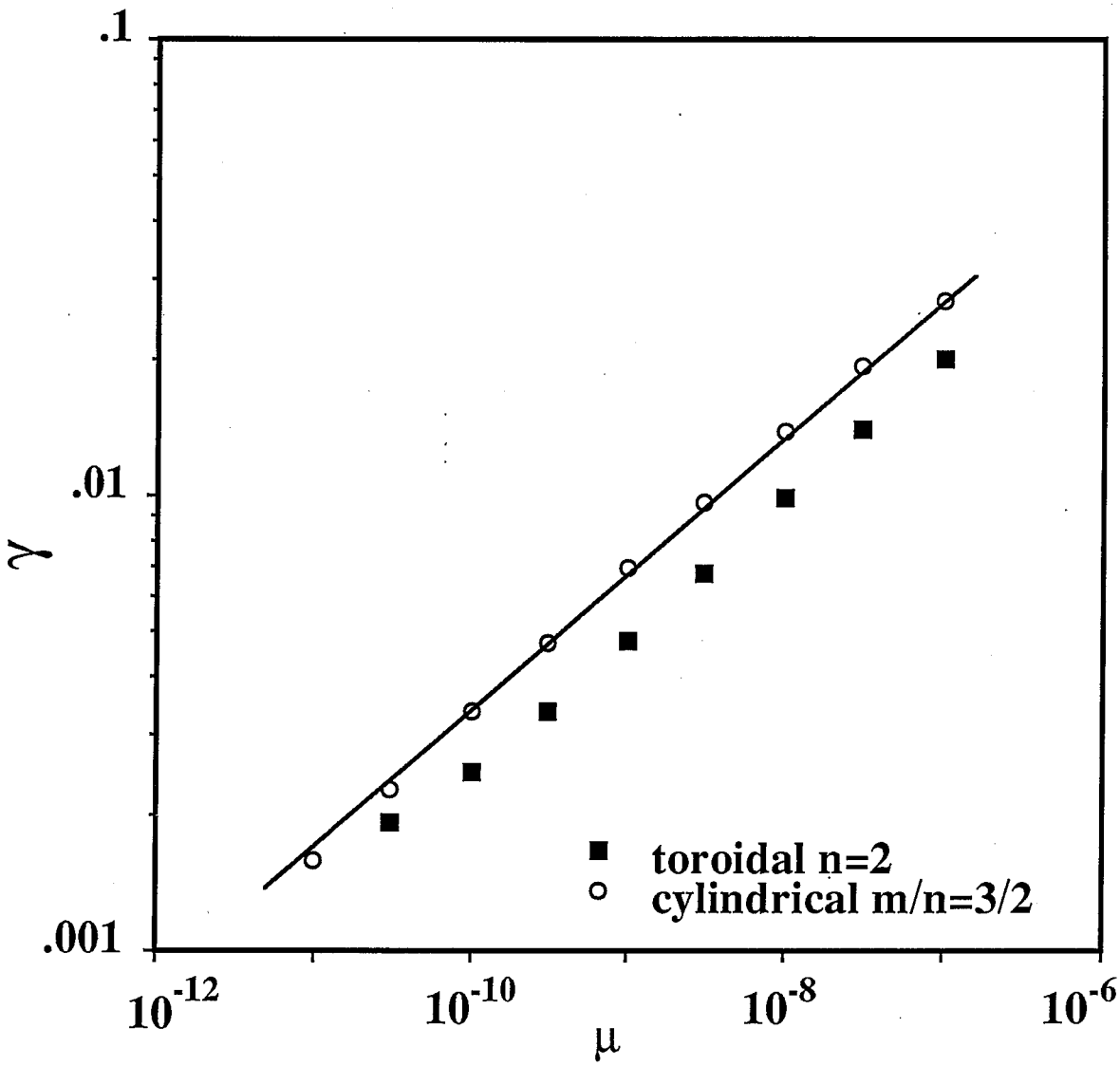

Fig. 1

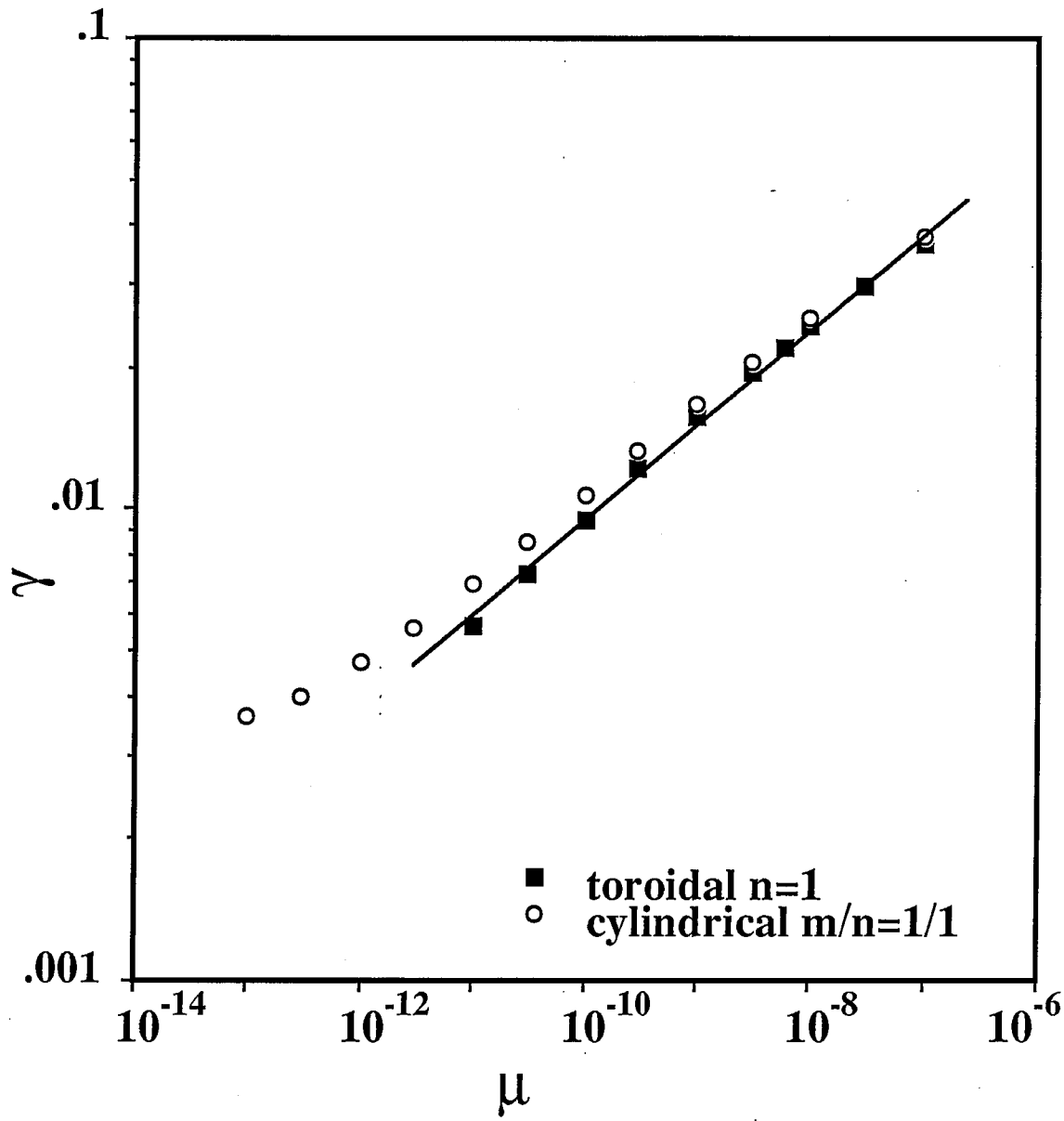
.1
.01
.001
γ
10^-14
10^-12
10^-10
10^-8
10^-6
μ
toroidal n=1
cylindrical m/n=1/1

Fig. 2

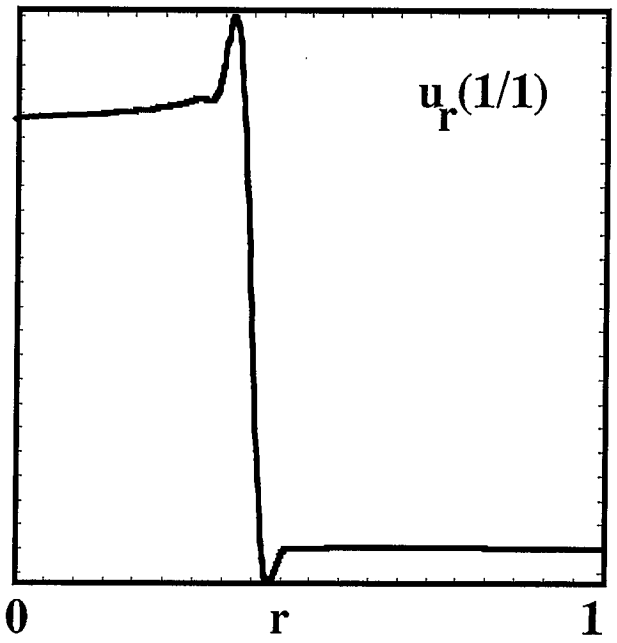

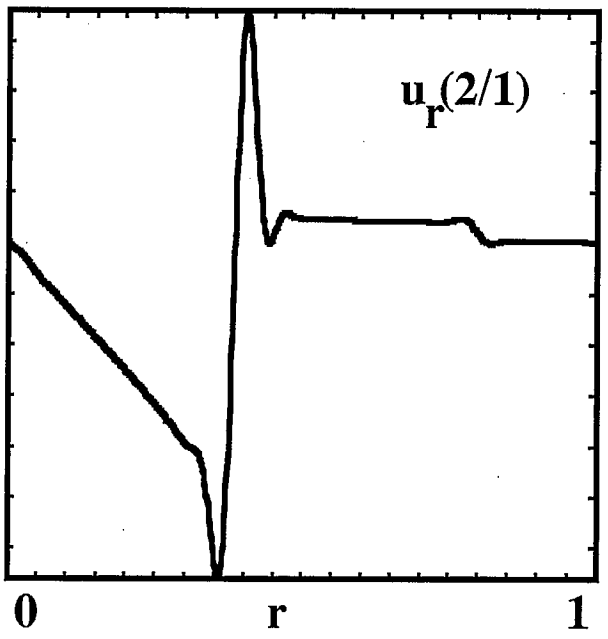

Fig. 3

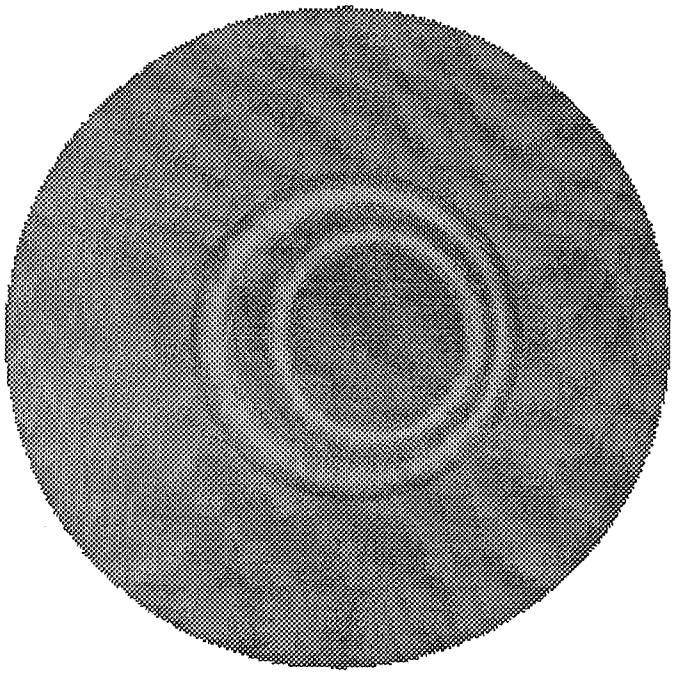

t = 706

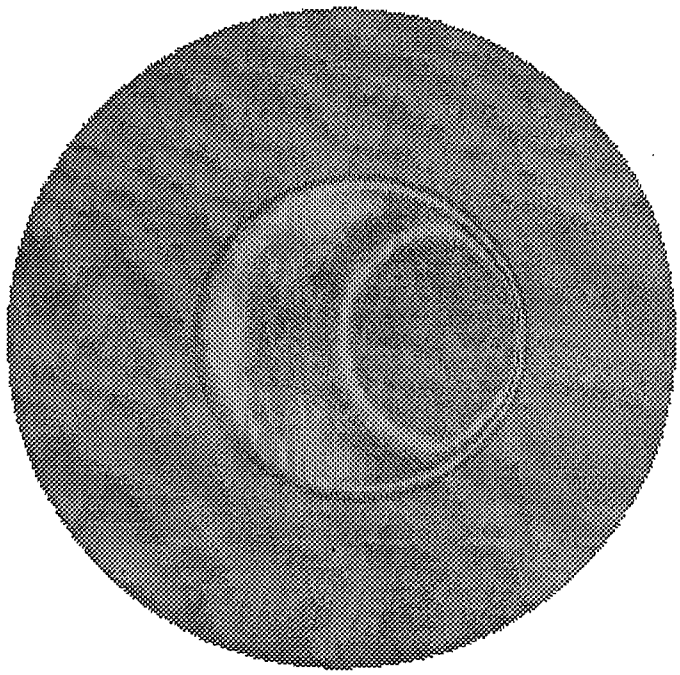

t = 1270

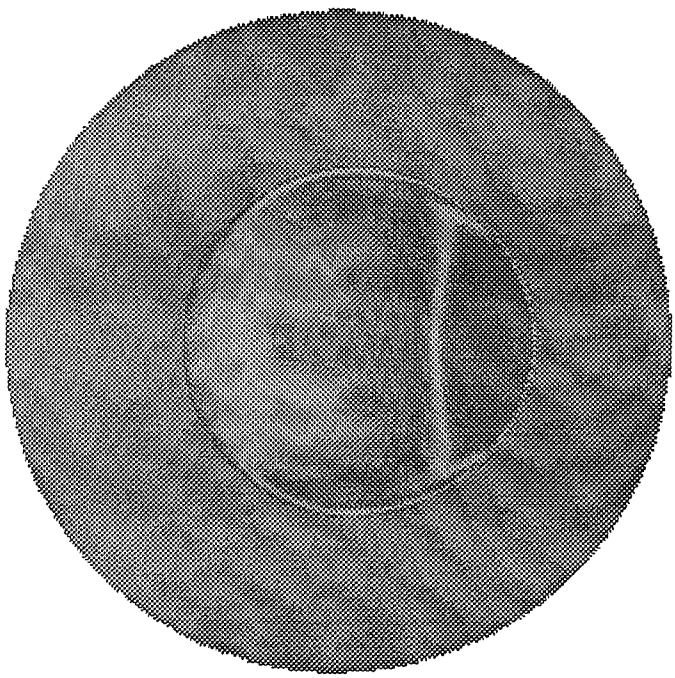

t = 1580

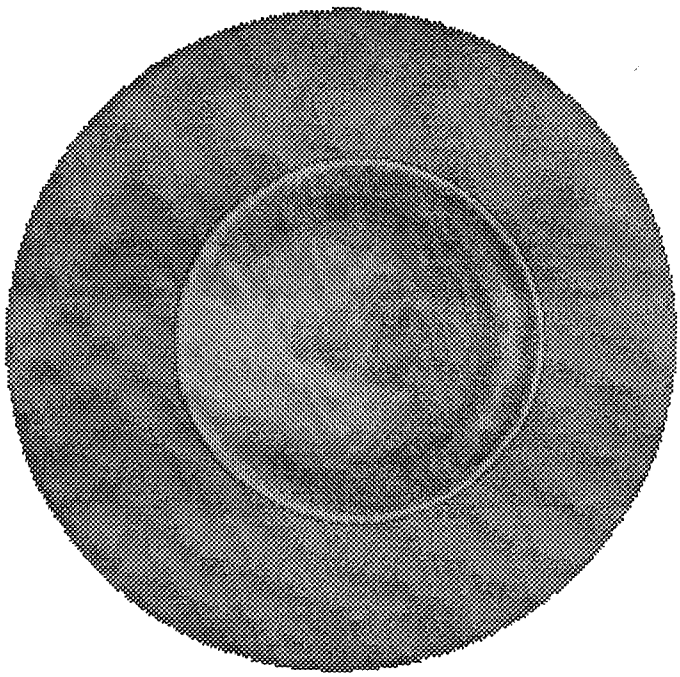

t = 1890

Fig. 4

t = 747

t = 1174

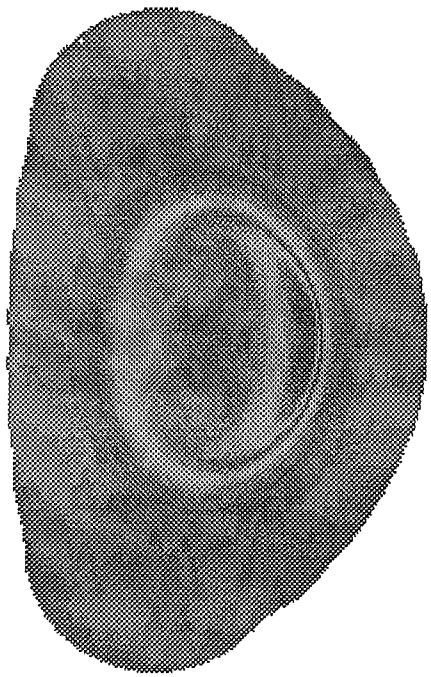

t = 1603

t = 2029

Fig. 5